JACS
JOURNAL OF THE AMERICAN CHEMICAL SOCIETY
ARTICLE
pubs.acs.org/JACS

Involvement of Carriers in the Size-Dependent Magnetic Exchange for Mn:CdSe Quantum Dots

Weiwei Zheng and Geoffrey F. Strouse*

Department of Chemistry and Biochemistry, Florida State University, Tallahassee, Florida 32306-4390, United States

S *Supporting Information*

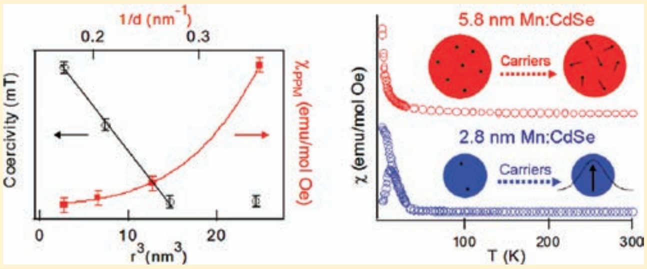

ABSTRACT: The magnetic behavior for Mn:CdSe (0.6%) quantum dots (QDs) exhibits size-dependent magnetic exchange mediated by the concentration of intrinsic carriers, which arise from surface states. High temperature paramagnetic behavior that can be fit to a Brillouin function with weak low temperature antiferromagnetic (AFM) coupling is observed for the large Mn:CdSe (5.0 and 5.8 nm) QDs. The 2.8 and 4.0 nm Mn:CdSe QDs display a size-independent blocking temperature (T_B) at 12 K, decreasing coercivity with increasing size, and a lowering of the activation barrier for spin relaxation as the QD is increased in size. The magnetic behavior is inconsistent with classical domain theory behavior for a superparamagnet (SPM) but can be accounted for in a carrier-mediated RKKY model. Fitting the susceptibility data reveals a Pauli-paramagnetic (PPM) component that is believed to arise from the presence of carriers. The carrier density is observed to scale with the surface to volume ratio in the QDs, indicating the carriers arise from surface states that are weakly localized resulting in the onset of long-distance carrier-mediated RKKY exchange inducing overall ferrimagnetism in the Mn:CdSe QDs when the carrier concentration is above a critical threshold.

INTRODUCTION

Dilute magnetic semiconductors (DMSs) are recognized as an important class of materials with potential for spin-based electronic and magneto-optical applications.[1−6] In DMS materials, Mn(II)-doped III−V semiconductors can exhibit ferromagnetism due to hole-mediated exchange interactions via the Ruderman−Kittel−Kasuya−Yosida (RKKY) model,[7,8] while in Mn(II)-doped II−VI compounds, the nearest neighbor antiferromagnetic exchange is observed.[5] The onset of ferromagnetic (FM) exchange has been achieved in p-type Mn(II)-doped II−VI compounds (Mn:CdTe, Mn:ZnTe),[9−11] as well as through photogenerated carriers in Mn:CdSe.[12] The results on II−VI DMS systems suggest that FM exchange can be achieved if exchange interactions in the II−VI materials can be enhanced via a carrier-mediated process.

The study of dilute magnetic semiconductors quantum dots (DMSQDs) based on CdSe is ideal for probing the fundamental interplay of charge, lattice, and magnetic degrees of freedom in quantum confined environments reflecting the exquisite control over the energies of the conduction and valence bands in these materials due to quantum confinement effects.[1,3,13,14] In addition, the participation of surface donor states in CdSe QDs due to ligation may lead to intrinsic carriers[15,16] that may induce a carrier-mediated process in these DMSQD systems. To date, only limited reports on FM exchange have been reported for Mn(II)-doped II−VI QDs.[17,18] In general, the limited reports reflect the difficulty in achieving intentional doping of paramagnetic ions into the core of a quantum dot (QD) due to the tenants of nucleation theory,[19] the high surface energies for ion addition to a growing QD facet,[13] and the propensity for QDs to exhibit self-annealing.[20] Although the difficulty of doping has been overcome by the use of predoped molecular clusters that act as critical nuclei for formation of the doped QDs,[2,3,17,21] allowing statistical incorporation of magnetic impurity ions onto the metal tetrahedral (T_d) sites, no studies have appeared investigating the size-dependent magnetic behavior for Mn:CdSe QDs. The exchange behavior will be influenced by QD size, dopant concentration, and the site of doping (core vs surface),[15,16,18] providing a carefully controlled study of size-dependent exchange in a DMSQD at a fixed dopant concentration, which is important for understanding the fundamental magnetic exchange in a well-defined environment.

In this Article, the size-dependent magnetic properties for 0.6% doped Mn:CdSe QDs passivated by dodecylamine are interrogated. The Mn:CdSe QDs are isolated as spherical, wurtzite nanocrystals with diameters of 2.8, 4.0, 5.0, and 5.8 nm. The doping level is constant throughout the samples due to the use of a predoped single source precursor and is confirmed by SQUID spin counting and X-ray fluorescence methods. In the Mn:CdSe QDs, paramagnetic (PM) behavior is observed for the 5.0 and 5.8 nm QDs, while a size-independent magnetic transition at 12 K and size-dependent coercivity are observed for the 2.8 and 4.0 nm QDs. The SQUID data for the larger QDs can be fit to a high temperature paramagnetic behavior exhibiting antiferromagnetic coupling at low temperature.

Received: January 18, 2011
Published: April 22, 2011

Analysis of the Curie−Weiss law plot for the 2.8 and 4.0 nm QDs indicates the participation of Pauli-paramagnetism (PPM) attributed to intrinsic carriers arising from surface states in the QDs generating ferromagnetic (FM) exchange below the blocking temperature. Consistent with the assignment of surface states producing carriers within the QD, a plot of the temperature-independent Pauli-paramagnetism versus QD size reveals a direct correlation between the observed magnetic moment and the QD size. It is believed the carriers in the smaller QDs mediate the exchange interaction in these single domain Mn:CdSe QDs, which leads to overall ferrimagnetism in the samples.

■ EXPERIMENTAL SECTION

Chemicals. Dodecylamine (DDA) (98+%, Alfa Aesar), $MnBr_2$ (anhydrous, 99%, Alfa Aesar), toluene (>99.9%, EMD Chemicals), and methanol (MeOH) (>99.8%, VWR) were used as supplied. $Li_4[Cd_{10}Se_4(SeC_6H_5)_{16}]$ (Cd_{10}) was prepared as described previously.[22]

Dodecylamine (DDA) Passivated Mn:CdSe (0.6%). DDA passivated Mn:CdSe (0.6%) with a 5−6% size distribution was prepared by the reaction between the single source precursor $Li_4[Cd_{10}Se_4(SeC_6H_5)_{16}]$ (Cd_{10}) and $MnBr_2$ in DDA, as described previously.[17,23] Briefly, the QDs are prepared by the dissolution of 200 mg (0.05 mmol) of Cd_{10} in ∼20 mL of DDA at 100 °C under N_2. To the solution was added 4.34 mg (0.02 mmol) of $MnBr_2$, and the reaction was allowed to stir for 1 h to induce ion exchange into the Cd_{10} cluster. The reaction mixture was heated to 220 °C (10 °C/min) inducing QD growth. The solution was cooled to room temperature, dissolved into ∼10 mL of toluene, precipitated by the addition of ∼15 mL of MeOH, and centrifuged to isolate the QDs (4×). The QDs were dissolved in a minimum of pyridine, precipitated (3×) by the addition of hexane to remove Mn(II) impurities, and isolated by centrifugation. Sequential dissolution/reprecipitation steps have been shown to effectively remove unreacted Mn(II).[17,20,21] QD size, morphology, and structure were analyzed by transmission electron microscopy (TEM) and confirmed with powder X-ray diffraction (pXRD) and UV−vis spectroscopy. The Mn doping level was analyzed by X-ray fluorescence (XRF) and was found to be 0.006 mol fraction (∼0.6%) relative to Cd for all of the samples.

Analysis. QD size, dispersity, and morphology were analyzed by TEM using a JEOL-2010 microscope operated at 200 kV. The QDs were dispersed on holey carbon (400 mesh) from a toluene solution. Size dispersities were measured by averaging ∼100 individual dots from the TEM. Optical absorption was analyzed in a 1 cm cell in toluene using a Cary 50 UV−vis spectrophotometer. The absorption maximum for the first exciton was used to estimate the QD size.[24] Powder X-ray diffraction was carried out on a Rigaku DMAX 300 Ultima 3 diffractrometer using Cu K_α (λ = 1.5418 Å) with the d-spacing calibrated to a Si standard to verify crystal motif.

Elemental composition analysis for Mn^{2+}, Cd^{2+}, and Se^{2-} was carried out in triplicate on an Oxford Instruments ED_{2000} X-ray fluorescence spectrometer with a Cu K_α source. The atomic concentration was measured for Mn^{2+} at 5.9 KeV, Cd^{2+} at 23.1 keV, and Se^{2-} at 11.2 keV. For a standard XRF measurement, the powdered samples were completely dissolved in 90% HNO_3, heated to remove excess NO_x, and then diluted to ∼3 mL with a 2% HNO_3 solution (to allow compatibility with the XRF sample holder). Calibration curves were generated using commercially prepared 1000 ppm elemental standards in 2% HNO_3, which results in accuracies of 5 ppm for Mn^{2+}, 3 ppm for Cd^{2+}, and 4 ppm for Se^{2-}.

Magnetic Measurements. Magnetic data on 20−40 mg of powdered samples of the QDs were measured on a Quantum Design MPMS XL7 SQUID magnetometer. Zero-field-cooled (ZFC) and field-cooled (FC, 0.01 T) measurements were collected for dc-susceptibility. The ac-susceptibility was measured between 1 and 1000 Hz. The temperature-dependent dc- and ac-magnetic susceptibility measurements were measured between 2 and 300 K. Field-dependent magnetization (M) data were collected between −7 and +7 T. The experimental data were fit to a Brillouin function, assuming $g = 2.0$, S is a variable, and the Mn(II) doping concentration in $Mn_xCd_{1-x}Se$ is $x = 0.006$.

■ RESULTS

The Mn:CdSe QDs were doped at 0.6% Mn(II) via the reaction of the "single-source" Mn(II)-doped $Li_4[Cd_{10}Se_4(SeC_6H_5)_{16}]$ (Cd_{10}), which allows consistent Mn(II) ion incorporation into the QD lattice for the studied sizes.[17] Growth of the QD is achieved at 220 °C, resulting in spherical, wurtzite QDs passivated by DDA with 5−6% size dispersity based on TEM. In Figure 1, the optical spectra, pXRD, and TEM data are shown for the isolated Mn:CdSe QDs. The optical absorption (Figure 1A) (dotted lines) and photoluminescence (PL) spectra (solid lines) can be fit to 2.8, 4.0, 5.0, and 5.8 nm in diameter for the isolated QDs. The color coding (2.8 nm (blue), 4.0 nm (green), 5.0 nm (black), and 5.8 nm (red)) for the experimental data is maintained throughout the text to simplify size identification for all experimental measurements. The sizes of the QDs measured by analysis of the optical data are confirmed by TEM analysis (Figure 1B). The concentration of Mn(II) in the CdSe QDs is on average 0.6% doping per QD as experimentally measured by XRF analysis and spin counting via SQUID magnetometry by fitting to Brillouin function, as described in the Supporting Information. The Mn(II) ion is assigned as a substitutional dopant on the Cd metal ion site based upon analysis of the total metal ion (Mn + Cd) to chalcogenide (Se) mole ratio, which yielded a value of 0.9:1 similar to the value observed for the undoped CdSe QD of 0.9:1. Consistent with an assignment of substitutional site occupation, the Mn(II) site is confirmed to be on a tetrahedral (T_d) symmetry site via the observation of two sextet hyperfine splitting patterns in EPR measurements arising from doping of the QD core and outermost QD layers (Supporting Information Figure 1). The Mn(II) doping will exhibit a Poisson distribution within the QD ensemble, but on average represents ∼2 Mn(II) ions in the 2.8 nm QD, ∼4 Mn(II) ions in the 4.0 nm QD, ∼7 Mn(II) ions in the 5.0 nm, and ∼10 Mn(II) ions in the QD in the 5.8 nm QD distributed statistically between the core and surface of the QD. The statistical distribution between surface and core of the QD is confirmed by analysis of the EPR spectra at high frequency (Supporting Information Figure 1).

Powder XRD (Figure 1C) allows assignment of a wurtzite crystal structure for the larger QDs, but can be interpreted as either cubic (zinc blende) or wurtzite for the smaller QDs. In QDs below 4 nm, the observation of a pseudo zinc blende pXRD pattern can be misinterpreted as a pure zinc blende structure because the presence of one to two stacking faults within the wurtzite Mn:CdSe QDs can lead to loss of the (110) reflection intensity at 45°.[25,26] Analysis of TEM-selected area electron diffraction (ED) data (Figure 1D) allows definitive assignment of wurtzite crystal morphology for all sizes of the Mn:CdSe based upon the observation of the (002), (110), and (201) reflections in the TEM-ED micrograph. The assignment of wurtzite crystal morphology from the TEM electron diffraction pattern suggests the loss of intensity for the 45° reflection in the pXRD is due to stacking faults in the small QDs as observed previously and not to formation of a zinc blende phase at this size scale.

In Figure 2A, the size-dependent zero-field-cooled (ZFC) and field-cooled (FC, 100 Oe) susceptibility (χ) plots for the Mn:

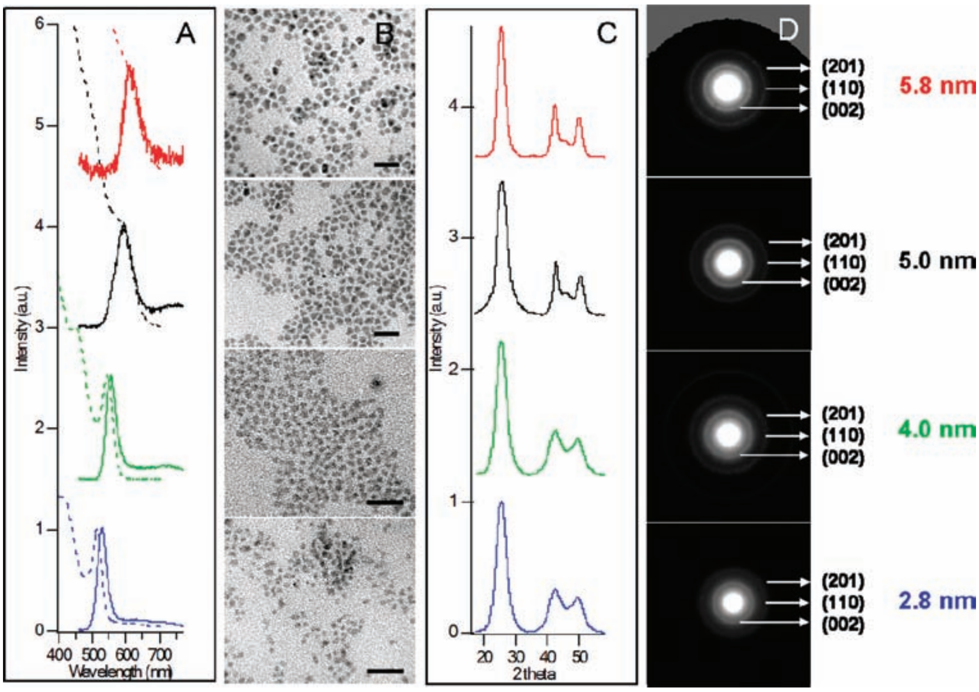

Figure 1. Characterization data for 2.8, 4.0, 5.0, and 5.8 nm (in diameter) 0.6% Mn:CdSe QDs: (A) absorption (dashed) and photoluminescence (solid) spectra, (B) TEM images (scale bar = 20 nm), (C) powder XRD patterns, and (D) TEM electron diffraction images. The figure is color coded for the QD sizes as noted in the image.

CdSe QDs measured by SQUID magnetometry are shown. The susceptibility plots are plotted relative to emu/mol of QD. The susceptibility plots for the 5.0 and 5.8 nm Mn:CdSe samples exhibit paramagnetic (PM) behavior, as expected for <1% doping levels in the Mn:CdSe samples.[5] The 2.8 and 4.0 nm Mn:CdSe samples show nonparamagnetic behavior with a clearly observed size-independent magnetic transition at 12 K. Field-dependent ZFC/FC SQUID measurements (Supporting Information Figure 2A) on the 2.8 nm Mn:CdSe at 50, 100, and 500 Oe indicate the 12 K magnetic transition is field independent. No transitions are observed for the 5.8 nm sample up to 100 Oe (Supporting Information Figure 2B). Temperature-dependent M versus H plots (Figure 2B) for the four samples indicate a saturation value (M_{SAT}) for the samples above 2 T that is size dependent but exhibits no clear correlation with QD size. The slower saturation may reflect the participation of spins at the QD surface.[27]

Size-dependent low temperature coercivity is observed for the 2.8 nm (0.29 T at 2 K) and 4.0 nm (0.16 T at 2 K) Mn:CdSe QDs in the M versus H plots below 20 K (Figure 2B and Supporting Information Figure 3). No coercivity is observed for the 5.0 and 5.8 nm Mn:CdSe samples. The coercivity in the small QDs decreases to 0 T near 20 K for the 2.8 and 4.0 nm Mn:CdSe QDs, which is typical for blocking temperature behavior observed for a superparmagentic (SPM) material. The experimental susceptibility curves are consistent with PM behavior in the 5.0 and 5.8 nm Mn:CdSe QD, while a more complex magnetic behavior reflective of SPM or spin-glass behavior is observed for the 2.8 and 4.0 nm Mn:CdSe QD samples. A plot of the temperature-dependent magnetization versus H/T (Supporting Information Figure 4) confirms the magnetization of the 5.0 and 5.8 nm Mn:CdSe can be described as PM. The susceptibility results on the 5.0 and 5.8 nm Mn:CdSe are consistent with theoretical predictions and experimental observations in bulk Mn:CdSe samples, where high temperature PM is reported with a weak antiferromagnetic (AFM) exchange at low T arising from the short-range exchange coupling between Mn(II) ions (J_{NN} (−7.3) and J_{NNN} (−2.4)).[5] The magnetic susceptibility plots for the 2.8 and 4.0 nm Mn:CdSe samples are more complex. As observed in Supporting Information Figure 4, a change in the magnetization is observed above 20 K when the magnetization data overlap in the M versus H/T plots for 2.8 and 4.0 nm QDs. The observed transition behavior is consistent with SPM-like character above a magnetic blocking temperature.[28]

Evidence of SPM behavior rather than spin-glass behavior in the 2.8 and 4.0 nm QDs can be further confirmed by measurement of the frequency-dependent ac-susceptibility. The phase behavior can be analyzed using the Mydosh criteria $\Phi = \Delta T_f/[T_f\Delta(\log \omega)]$, where T_f is the temperature at which the maximum in $\chi'(T)$ occurs, ΔT_f is the difference in T_f between an initial frequency ω_i and final frequency ω_f, and $\Delta(\log \omega)$ is the difference between the log of the initial and final measuring frequencies.[29] A value of Φ observed for SPM materials is $\Phi = 10^{-1}-10^{-2}$, while a spin glass yields a value of $<10^{-2}$.[29] Using the Mydosh parameter, SPM character has been assigned to Fe_3O_4 nanocrystals ($\Phi = 0.07$)[30] and an Fe−Ni alloy ($\Phi = 0.1$),[29] while spin glass behavior is observed for $Zn_{1-x}Mn_xIn_2Te_4$ ($\Phi = 0.005$).[31] The ac-susceptibility of the 2.8 and 4.0 nm Mn:CdSe QDs was measured at 1, 10, 100, and 1000 Hz (Figure 3). In Figure 3, a plot of the real (χ') (Figure 3A) and imaginary (χ'') (Figure 3B) components reveals a phase lag in the magnetic data, which can arise from either superparamagnetic (SPM) or spin-glass (SG) behavior in the QDs. The values of Φ obtained for 2.8 and 4.0 nm dots are 0.09 and 0.08, respectively, and confirm the assignment of SPM behavior in the 2.8 and 4.0 nm Mn:CdSe samples.[30] SPM behavior has been observed previously in 4.0 nm Mn(1%):CdSe QDs.[17]

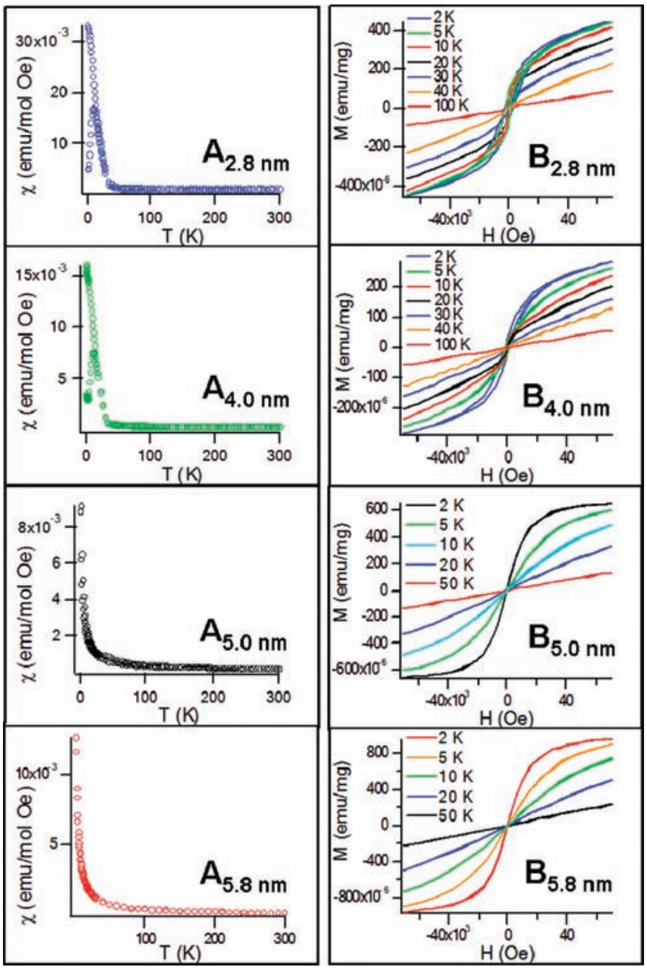

Figure 2. (A) Temperature-dependent ZFC and FC (100 Oe) susceptibility data, and (B) temperature-dependent field sweep plots for 2.8, 4.0, 5.0, and 5.8 nm 0.6% Mn:CdSe QDs.

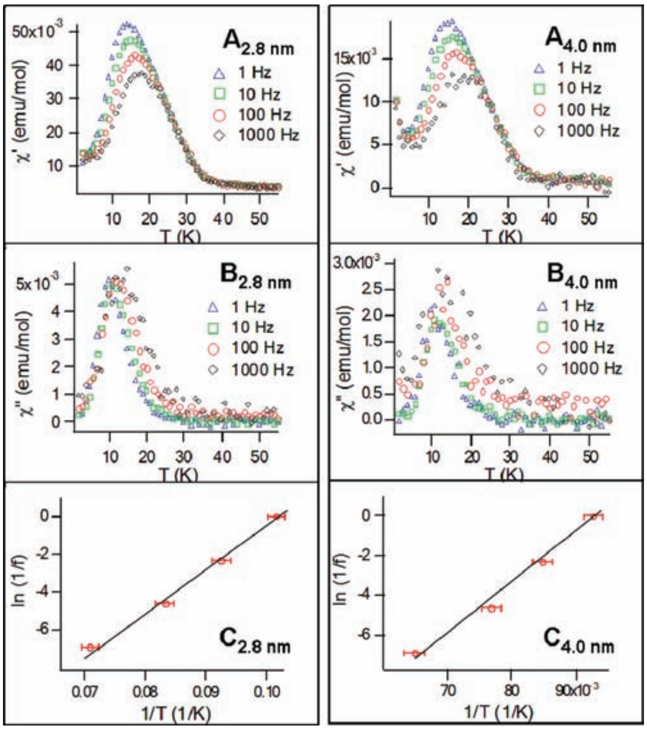

Figure 3. Temperature-dependent ac-susceptibility (1−1000 Hz) data for the 2.8 and 4.0 nm 0.6% Mn:CdSe QDs showing the (A) in-phase (real) component $\chi'(T)$, (B) out-of-phase (imaginary) component $\chi''(T)$, and (C) temperature-dependent Arrhenius plots for the imaginary component $\chi''(T)$.

The energy barrier for spin relaxation can be extracted from the temperature-dependent ac-susceptibility curves (Figure 3C). Fitting the data to the Arrhenius equation, $\ln(\tau/\tau_0) = E_a/(k_BT)$, where τ is the average relaxation time corresponding to the frequency of the ac measurement and E_a/k_B is the energy barrier to magnetic reversal in an isolated particle, yields a value for the 2.8 nm Mn:CdSe QDs of τ_0 (2.8 nm) = 9.6×10^{-11} s and E_a/k_B (2.8 nm) = 225 ± 10 K ($E_a = 4.9 \times 10^{-40}$ eV), and a value for the 4.0 nm Mn:CdSe QDs of τ_0 (4.0 nm) = 6.6×10^{-11} s and E_a/k_B (4.0 nm) = 250 ± 10 K ($E_a = 5.5 \times 10^{-40}$ eV). The value of τ_0 for both 2.8 and 4.0 nm QDs is in the range observed for SPM materials ($\tau_0 = 10^{-9}-10^{-11}$ s).[30]

The magnetization data for the 5.0 and 5.8 nm Mn:CdSe QDs exhibit the predicted high temperature PM behavior for the low doping levels of Mn(II) in CdSe.[5] The observation of SPM-like behavior in the 2.8 and 4.0 nm QDs with an observed magnetic phase transition at 12 K coupled to the onset of a magnetic hysteresis is surprising. A plot of the coercivity data versus temperature in Figure 4A illustrates that although the T_B is size independent, the coercivity at 2 K is size dependent for the 4.0 and 2.8 nm Mn:CdSe samples. A plot of the coercivity versus size (Figure 4A inset) shows a decreasing linear correlation with increasing volume of the QD up to the 5.0 nm sample. The coercivity behavior is inconsistent with Domain theory for SPM materials, because classical SPM behavior would predict an increasing coercivity as the critical domain size is approached. According to the Stoner−Wohlfarth theory, the magnetocrystalline anisotropy E_a of a single domain particle should decrease with decreasing particle size, because $E_a = KV \sin^2 \theta$, where K is magnetocrystalline anisotropy constant, V is the volume of the nanoparticle, and θ is the angle between the magnetization direction and the easy axis of the nanoparticle.[32,33] Assuming the values of K and θ are constants, the Stoner−Wohlfarth theory predicts for the Mn:CdSe QDs a decrease in E_a from 250 K (4.0 nm) to 86 K (2.8 nm) (the E_a for 2.8 nm QD is predicted from theory to decrease by 34.3% of the value for the 4.0 nm QD) to account for the decrease in volume at constant Mn concentration. For the Mn:CdSe samples in the <4.0 nm size regime, however, the measured values for the energy barrier and relaxation lifetime are size independent within experimental error, which is inconsistent with the magnetization behavior arising from simple domain theory predictions. The failure to follow simple domain theory predictions may reflect contributions from surface-induced carriers, which would increase with decreasing QD size, the inverse of the predicted domain theory behavior for a SPM system.

■ DISCUSSION

The observation of the size-dependent magnetic behavior of the Mn:CdSe DMSQD sample is surprising. The exchange interaction in Mn:CdSe in the absence of carriers involves primarily Mn−Mn nearest neighbor exchange interactions, leading to antiferromagnetic (AFM) exchange.[5] At a doping level of 0.6% Mn(II) ($x = 0.006$ in $Mn_xCd_{1-x}Se$), the Mn(II)

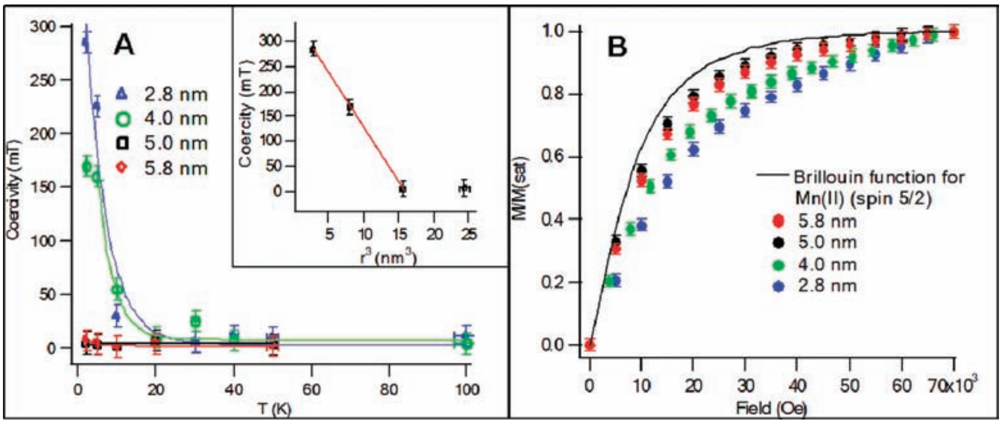

Figure 4. Plot of the (A) temperature-dependent coercive field (mT) for 2.8, 4.0, 5.0, and 5.8 nm Mn:CdSe QDs. The dependence of the coercive at 2 K versus volume of the QD is plotted in the inset. (B) Theoretical Brillouin function assuming $S = 5/2$, $g = 2.0$ as compared to the normalized magnetization data.

separation distance should approach a theoretically calculated mean value of 2.1 ± 0.6 nm assuming a Poisson distribution of doping. The large separation distance for Mn(II) centers should lead to PM behavior for all of the samples with no observable magnetic transition above 1 K.[5] An assumption of the magnetic exchange in the Mn:CdSe DMSQD of a simple Mn(II)−Mn(II) nearest neighbor exchange interaction cannot account for the observation of size-dependent ferromagnetic (FM) exchange in the Mn:CdSe QDs in this study.

Ferromagnetic exchange can arise from formation of spin clusters at high doping levels, as previously reported;[17] however, at 0.6% doping levels within a 2.8 nm Mn:CdSe QD, only two Mn(II) ions would be present, and a calculation of spin-cluster formation at <1% suggests the magnetic behavior cannot be easily attributed to spin-cluster formation in this doping and size regime. An alternative possibility is the presence of intrinsic carriers in the Mn:CdSe DMSQD arising from the nonstoichiometric Cd to Se ratios[34] or the presence of ligand-induced states at the QD surface.[15,16] The presence of weakly localized or delocalized carriers can result in the observation of magnetic exchange via a carrier-mediated process in PbSnMnTe,[35] where intrinsic carriers arise from nonstoichiometric Te content. The carrier-mediated RKKY process in PbSnMnTe leads to FM exchange over a narrow carrier density range, with PM behavior for $p < 3 \times 10^{20}$ cm^{-3} and FM behavior reported for $p > 3 \times 10^{20}$ cm^{-3}.[35] Although carriers have not been invoked to describe magnetic exchange in Mn:CdSe QDs previously, in undoped CdSe QDs generation of intrinsic carriers has been reported to arise from surface states.[15,16] The presence of hole carriers in CdSe QDs may explain the various reports of magnetic behavior in magnetically doped CdSe QDs where ferromagnetic, spin-glass, and paramagnetic have been reported depending on the doping level and QD size.[17,21]

For surface-induced carriers, an increase in carrier density is anticipated to follow the surface to volume ratio for the QD, which changes dramatically below 4 nm in diameter.[35,36] The size-dependent carrier density in the Mn:CdSe QD samples in this study can be analyzed by fitting the normalized magnetization plots for the various QD sizes to extract the concentration of the temperature-dependent and temperature-independent spins (Figure 4B and Supporting Information Figure 5). The spin density is analyzed by fitting the field-dependent SQUID data to a Brillouin function (eq 1a) to estimate the spin moment per Mn ion, where the Brillouin function (eq 1b) can be written as

$$M = Ng\mu_B J B_J(\eta) \qquad (1a)$$

$$B_J(\eta) = \frac{2J+1}{2J}\coth\left(\frac{2J+1}{2J}\eta\right) - \frac{1}{2J}\coth\left(\frac{1}{2J}\eta\right) \qquad (1b)$$

$$\eta = \frac{g\mu_B H}{k_B T} \qquad (1c)$$

where N is the molar volume, μ_B is the Bohr magneton, g is the free electron Landé g-value, and J is the spin. To fit the magnetization, the Brillouin function is used with η (eq 1c) being equal to the ratio between the spin components and the thermal energy, where H is the applied magnetic field and k_B is Boltzmann's constant. Equation 1a is fit by allowing the values for J to float with $g = 2.0$. The results reveal the magnetization behavior is size dependent with the 2.8 nm QD showing slower saturation than predicted for a theoretical fit to a $S = 5/2$ ($L = 0$ for Mn(II) ion), $g = 2.0$ system. The lower slope for the Brillouin function indicates a lowering of the total spin moment in the QD sample than theoretically predicted for a Mn(II) center. As the QD size increases (5.0 and 5.8 nm), the saturation behavior approaches the theoretical plot, indicating the observed spin moment is consistent with the theoretical prediction for Mn(II) centers within the QD.

In Supporting Information Figure 5, the temperature-dependent fit of the Brillouin function for the 2.8 nm (2, 40, and 100 K), 4.0 nm (2, 40, and 100 K), 5.0 nm (2 and 50 K), and 5.8 nm (2 and 50 K) Mn:CdSe QD is shown. The Brillouin fit of the 2.8 and 4.0 nm Mn:CdSe QD at 2 K does not follow the theoretically predicted behavior (shape and total spin magnetic momentum) for a $S = 5/2$ Mn(II) dopant (2.8 nm ($S = 1.4$), 4.0 nm ($S = 1.0$)) for the doping levels measured by XRF. At 100 K, the 2.8 nm QD can be fit to $S = 2.5$ as theoretically predicted for the Mn(II) ion, while the 4.0 nm is fit to $S = 2.2$. The lower value for S than theoretically predicted in the 4.0 nm data at 100 K is believed to reflect experimental error due to a small sample size for the SQUID measurements, leading to the necessity of a large diamagnetic correction to the original SQUID data for this sample. The Brillouin analysis of the 5.0 and 5.8 nm QD shows

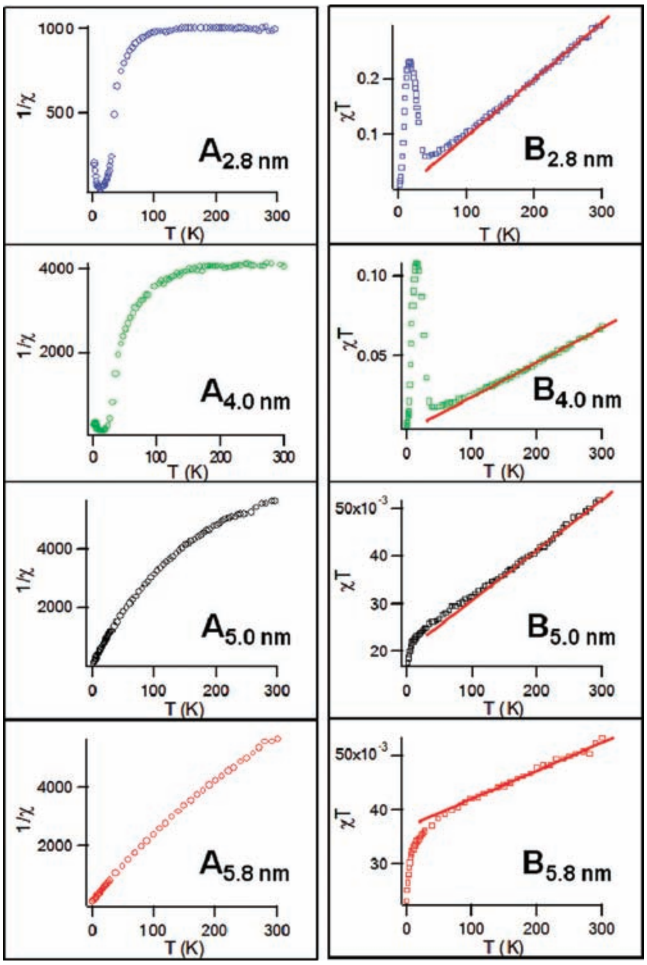

Figure 5. Size-dependent (A) Curie–Weiss law and (B) χT versus T plots for Mn:CdSe QDs.

the magnetization behavior is close to the theoretical value of $S = 5/2$ for both samples at 2 and 50 K. The fits indicate the Mn(II) centers conserve their spin magnetic momentum of 5 Bohr magneton for the large QDs (2 and 50 K) and for the small QDs at >40 K, but exhibit low spin magnetic moment and a poor Brillouin fit at 2 K for the small QDs (2.8 and 4.0 nm QDs). A decrease in the value of spin magnetic moment with decreasing volume but increasing magnetic exchange interactions (coercivity) supports the assumption of potential surface-induced contributions to the total magnetization behavior in these materials, where carriers AFM couple to the Mn(II) spins in the lattice at low-T for the small QDs.

In Figure 5A, a Curie–Weiss (C–W) law susceptibility plot of the temperature-dependent SQUID data, $1/\chi = (T - \theta)^*C^{-1}$ (C is the Curie constant, T is temperature in Kelvin, and θ is the Curie temperature), deviates from classical Curie–Weiss behavior for all sizes of Mn:CdSe, exhibiting a temperature-dependent paramagnetic and a temperature-independent Pauli-paramagnetic contribution to the susceptibility data. Because the temperature-independent term is size dependent with a decreasing contribution to the magnetization data with increasing QD size, the data for the 2.8 and 4.0 nm cannot be fit to C–W behavior. A fit of the data for the 5.0 and 5.8 nm Mn:CdSe reveals high temperature PM behavior where a negative Curie temperature is indicative of AFM exchange with a θ of −4.7 K (5.8 nm) and −11.8 K (5.0 nm). The negative Curie temperature (θ) is indicative of AFM exchange interactions in the lattice. The negative deviation for the low-T susceptibility data in Figure 5A can be interpreted in terms of a ferrimagnetic phase behavior in the Mn:CdSe DMSQDs.[37]

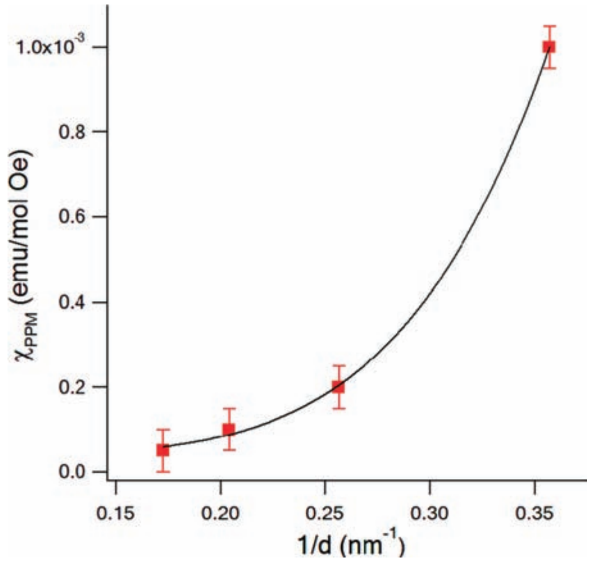

Figure 6. The size-dependent magnetic susceptibility arising from the temperature-independent Pauli-paramagnetic contribution to the total susceptibility.

Extraction of the temperature-independent Pauli-paramagnetic (PPM) component from the susceptibility data in Figure 2 can be achieved using a modified Curie–Weiss plot (Figure 5B), because $\chi_{\text{exptl}}T = C + \chi_{\text{PPM}}T$. In Figure 5B, the PPM contribution is extracted from the slope of the plot at high temperature, while the Curie constant can be extracted from the y-intercept. The measured Curie constants for the samples are 4.3 emu·K/(mol·Oe) (5.8 nm), 2.8 emu·K/(mol·Oe) (5.0 nm), 0.9 emu·K/(mol·Oe) (4.0 nm), and 0.6 emu·K/(mol·Oe) (2.8 nm), which does not agree with the theoretically value of 4.4 (emu·K/mol) for $S = 5/2$ except for the largest QD. The Curie constant (C) is reported in terms of the emu per mole of Mn(II) ion in the sample from the χ_{exptl} data.

The strongest PPM contribution to the susceptibility data is observed for the 2.8 nm QD, with decreasing PPM contributions as the QD increases in size. Assuming the susceptibility for the PPM arises only from intrinsic carriers, the PPM susceptibility can be related to the concentration of carriers within the QD, implying as the QD decreases in size the carrier concentration per unit volume increases. In Figure 6, a plot of the carrier concentration versus inverse QD diameter shows an exponential dependence on the PPM concentration with size. The inverse dependence on diameter in Figure 6 suggests the decrease in carrier density reflects the surface to volume ratio for the QD, as suggested in earlier SQUID and XMCD measurements.[15,16] Although the experimental observation is consistent with carrier density measured for CdSe QDs and the reported increase in carrier concentration in CdSe with decreased QD size, it cannot distinguish between donor levels generated by the ligand, the Cd to Se ratio, or a combination of the two.[15,16,34]

■ CONCLUSION

The $1/d$ dependence of the PPM contributions to the susceptibility data supports the presence of intrinsic carriers in the Mn:CdSe QDs, which are likely associated with surface states.

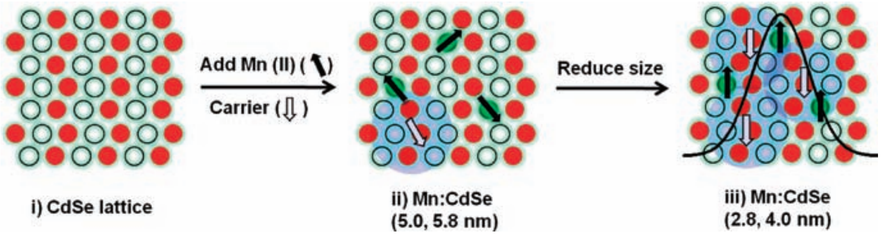

Figure 7. Proposed model of the onset of magnetic exchange in Mn:CdSe QDs governed by long-range carrier-mediated RKKY processes.

The presence of carriers generates electron density at the Fermi level, as suggested in earlier studies on CdSe QDs,[15,16] which leads to indirect carrier-mediated RKKY interaction as described in Figure 7. Increasing carrier densities with decreasing QD size leads to the onset of SPM DMSQD exhibiting a magnetic transition at 12 K for the 2.8 and 4.0 nm QDs. The onset of magnetization below 4.0 nm where the susceptibility data exhibit blocking behavior reflects the critical threshold for the carrier density to induce the exchange interactions within a SPM-like single domain (Figure 7). The magnetization study for Mn:CdSe QD suggests with an increase in size the reduction in surface to volume ratio lowers the carrier density below the critical threshold due to the decrease in ligand-induced surface states per QD volume. The larger QDs exhibit paramagnetic behavior when the carrier density is below the percolation threshold in the 5.0 and 5.8 nm Mn:CdSe DMSQDs.

The surface-induced carriers, which are believed to arise from charge transfer effects associated with the ligation layer, must be weakly localized to result in the long-range RKKY exchange coupling. The long-distance carrier-mediated exchange coupling attributed to AFM exchange between Mn(II) spins and weakly bound carriers, as proposed by MacDonald et al.,[36] generates ferrimagnetic phase behavior in the QDs below 4.0 nm in diameter. The participation of carrier-mediated exchange would explain the decreased magnetic saturation value observed for the smallest QDs (Figure 2). Similar behavior has been reported for ligand-induced carrier-mediated exchange in Mn(II)-doped ZnO QDs[18] and in semimagnetic II—VI bulk semiconductors.[11,35,38] Further studies investigating the ligand dependent influence on the magnetic susceptibility are underway to deduce the importance of ligand passivation on the observed magnetic properties.

■ ASSOCIATED CONTENT

Ⓢ Supporting Information. EPR measurements for 2.8 nm and 5.8 nm Mn:CdSe QDs, individual field sweep SQUID measurements for the 2.8 and 4.0 nm Mn:CdSe samples, the field-dependent zero-field-cooled (ZFC) and field-cooled (FC) SQUD data for the 2.8 and 5.8 nm Mn:CdSe QDs, the magnetization versus H/T plots for the samples, and the temperature-dependent Brillouin function fits. This material is available free of charge via the Internet at http://pubs.acs.org.

■ AUTHOR INFORMATION

Corresponding Author

strouse@chem.fsu.edu

■ ACKNOWLEDGMENT

We wish to thank NSF-CHE-0911080 and NSF-DMR-0701462 for financial support, acknowledge contributions from Dr. Michael Shatruk and Dr. Peng Xiong with regards to the magnetic behavior, and thank Dr. Yan Xin for performing and analyzing the TEM measurement at the National High Magnetic Field Laboratory. The NHFML is supported by the NSF Cooperative Agreement No. DMR-0654118 and by the State of Florida.

■ REFERENCES

(1) Erwin, S. C.; Zu, L.; Haftel, M. I.; Efros, A. L.; Kennedy, T. A.; Norris, D. J. *Nature* **2005**, *436*, 91–94.

(2) Yu, J. H.; Liu, X.; Kweon, K. E.; Joo, J.; Park, J.; Ko, K.-T.; Lee, D. W.; Shen, S.; Tivakornsasithorn, K.; Son, J. S.; Park, J.-H.; Kim, Y.-W.; Hwang, G. S.; Dobrowolska, M.; Furdyna, J. K.; Hyeon, T. *Nat. Mater.* **2010**, *9*, 47–53.

(3) Bryan, J. D.; Gamelin, D. R. *Prog. Inorg. Chem.* **2005**, *54*, 47–126.

(4) Jaworski, M. C.; Yang, J.; Mack, S.; Awschalom, D. D.; Heremans, J. P.; Myers, R. C. *Nat. Mater.* **2010**, *9*, 898–903.

(5) Furdyna, J. K. *J. Appl. Phys.* **1988**, *64*, R29–R64.

(6) Ohno, H. *Science* **1998**, *14*, 951–956.

(7) Dietl, T.; Ohno, H.; Matsukura, F. *Phys. Rev. B* **2001**, *63*, 195205.

(8) Dietl, T. *Nat. Mater.* **2010**, *9*, 965–974.

(9) Haury, A.; Wasiela, R.; Arnoult, A.; Cibert, J.; Tatarenko, S.; Dietl, T.; Merle d'Aubigné, Y. *Phys. Rev. Lett.* **1997**, *79*, 511–514.

(10) Ferrand, D.; Cibert, J.; Bourgognon, C.; Tatarenko, S.; Wasiela, A.; Fishman, G.; Bonanni, A.; Sitter, H.; Koleśnik, S.; Jaroszyński, J.; Barcz, A.; Dietl, T. *J. Cryst. Growth* **2000**, *214—215*, 387–390.

(11) Dietl, T.; Sawicki, M.; Van Khoi, L.; Jaroszyski, J.; Kossacki, P.; Cibert, J.; Ferrand, D.; Tatarenko, S.; Wasiela, A. *Phys. Status Solidi B* **2002**, *229*, 665–672.

(12) Junnarkar, M. R.; Alfano, R. R.; Furdyna, J. K. *IEEE J. Quantum Electron.* **1988**, *24*, 315–324.

(13) Norris, D. J.; Efros, A. L.; Erwin, S. C. *Science* **2008**, *319*, 1776–1779.

(14) Brus, L. E. *J. Chem. Phys.* **1984**, *80*, 4403–4409.

(15) Meulenberg, R. W.; Lee, J. R. I.; McCall, S. K.; Hanif, K. M.; Haskel, D.; Lang, J. C.; Terminello, L. J.; van Buuren, T. *J. Am. Chem. Soc.* **2009**, *131*, 6888–6889.

(16) Neeleshwar, S.; Chen, C. L.; Tsai, C. B.; Chen, Y. Y.; Chen, C. C.; Shyu, S. G.; Seehra, M. S. *Phys. Rev. B* **2005**, *71*, 201307(R).

(17) Magana, D.; Perera, S. C.; Harter, A. G.; Dalal, N. S.; Strouse, G. F. *J. Am. Chem. Soc.* **2006**, *128*, 2931–2939.

(18) Kittilstved, K. R.; Gamelin, D. R. *J. Am. Chem. Soc.* **2005**, *127*, 5292–5293.

(19) Beaulac, R.; Archer, P. I.; Ochsenbein, S. T.; Gamelin, D. R. *Adv. Funct. Mater.* **2008**, *18*, 3873–3891.

(20) Mikulec, F. V.; Kuno, M.; Bennati, M.; Hall, D. A.; Griffin, R. G.; Bawendi, M. G. *J. Am. Chem. Soc.* **2000**, *122*, 2532–2540.

(21) Hanif, K. M.; Meulenberg, R. W.; Strouse, G. F. *J. Am. Chem. Soc.* **2002**, *124*, 11495–11502.

(22) Lovingood, D. D.; Achey, R.; Paravastu, A. K.; Strouse, G. F. *J. Am. Chem. Soc.* **2010**, *132*, 3344–3354.

(23) Meulenberg, R. W.; van Buuren, T.; Hanif, K. M.; Willey, T. M.; Strouse, G. F.; Terminello, L. *Nano Lett.* **2004**, *4*, 2277–2285.

(24) Qu, L.; Peng, X. *J. Am. Chem. Soc.* **2002**, *124*, 2049–2055.

(25) Bawendi, M. G.; Kortan, A. R.; Stiegerwald, M. L.; Brus, L. E. *J. Chem. Phys.* **1989**, *91*, 7282–7290.

(26) Murray, C. B.; Norris, D. J.; Bawendi, M. G. *J. Am. Chem. Soc.* **1993**, *115*, 8706–8715.

(27) Kodama, R. H. *J. Magn. Magn. Mater.* **1999**, *200*, 359–372.

(28) Bean, C. P.; Livingston, J. D. *J. Appl. Phys.* **1959**, *30*, 120S–129S.

(29) Culp, J. T.; Park, J. H.; Meisel, M. W.; Talham, D. R. *Inorg. Chem.* **2003**, *42*, 2842–2848.

(30) Goya, G. F.; Berquó, T. S.; Fonseca, F. C.; Morales, M. P. *J. Appl. Phys.* **2003**, *94*, 3520–3528.

(31) Goya, G. F.; Sagredo, V. *Phys. Rev. B* **2001**, *64*, 235208.

(32) Stoner, E. C.; Wohlfarth, E. P. *Philos. Trans. R. Soc. London, Ser. A* **1948**, *240*, 599–642.Reprinted in *IEEE Trans. Magn.* **1991**, *27*, 3475—3518.

(33) Liu, C.; Zhang, Z. J. *Chem. Mater.* **2001**, *13*, 2092–2096.

(34) Jasieniak, J.; Mulvaney, P. *J. Am. Chem. Soc.* **2007**, *129*, 2841–2848.

(35) Story, T.; Galazka, R. R.; Frankel, R. B.; Wolff, P. A. *Phys. Rev. Lett.* **1986**, *56*, 777–779.

(36) Abolfath, M.; Jungwirth, T.; Brum, J.; MacDonald, A. H. *Phys. Rev. B* **2001**, *63*, 054418.

(37) Spaldin, N. A. *Magnetic Materials: Fundamentals and Device Applications*; Cambridge University Press: UK, 1969; pp 107—113.

(38) Galazka, R. R. *Phys. Status Solidi B* **2006**, *243*, 759–767.